RESEARCH ARTICLE | JANUARY 15 2026

Giant magnetostrains in MnFe(P,Si,B)/epoxy composites at intermediate magnetic fields

B. Huhe ; H. Yibole ; F. Guillou ; N. H. van Dijk ; E. Brück

APL Mater. 14, 011107 (2026)
https://doi.org/10.1063/5.0307815

Giant magnetostrains in MnFe(P,Si,B)/epoxy composites at intermediate magnetic fields

Cite as: APL Mater. 14, 011107 (2026); doi: 10.1063/5.0307815
Submitted: 18 October 2025 • Accepted: 15 December 2025 •
Published Online: 15 January 2026

B. Huhe,[1] H. Yibole,[1] F. Guillou,[1,2,a)] N. H. van Dijk,[3] and E. Brück[3]

AFFILIATIONS

[1] College of Physics and Electronic Information, Inner Mongolia Key Laboratory of Applied Condensed Matter Physics, Inner Mongolia Normal University, 81 Zhaowuda Rd, Hohhot 010022, China
[2] Normandie University, ENSICAEN, UNICAEN, CNRS, CRISMAT, Caen 14000, France
[3] FAME Group, Department of Radiation Science and Technology, Delft University of Technology, Mekelweg 15, 2629 JB Delft, The Netherlands

[a)] **Author to whom correspondence should be addressed:** francois.guillou@unicaen.fr

ABSTRACT

Magnetostrictive materials are widely used in actuators, sensors, and energy-harvesting systems, but many high-performance compounds rely on heavy rare-earth elements or require high magnetic fields to develop giant magnetostrains. Here, we present Fe_2P/epoxy composites, exploiting an anisotropic first-order ferromagnetic transition (FOMT) to generate giant magnetostrains. A parametric model based on structural discontinuities and thermodynamic considerations is proposed to guide composition selection. Textured $MnFe_{0.95}P_{0.55}Si_{0.40}B_{0.05}$/epoxy composites were prepared by magnetic field alignment and characterized by strain-gauge dilatometry measurements as a function of temperature and magnetic field. Near the FOMT, despite matrix dilution effects, linear magnetostrains up to 0.22% at 2 T (0.37% at 7 T) are achieved. In particular, at intermediate fields, the magnetostrain shows a nearly linear increase with the field of about 0.1%/T (1000 ppm/T) with limited hysteresis. These results demonstrate that Fe_2P-type compounds, previously developed for magnetocaloric applications, can be adapted into scalable, low-cost magnetostrictive composites with tunable transition temperatures that rely only on abundant elements.

I. INTRODUCTION

Magnetostrains correspond to the relative length change of a material induced by an applied magnetic field, arising from mechanisms such as magnetic domain reorientation, magnetocrystalline anisotropy, phase transitions, or twin boundary motion. Magnetostrictive materials have attracted significant attention due to their broad range of applications, including actuators and sensors (motion, stress, or torque detection), ultrasonic transducers (sonar and medical imaging), as well as energy harvesting and vibration control systems. These applications rely on the interconversion between magnetic and mechanical energy, and in most cases, the performance can be greatly enhanced by stronger magnetostrictive effects.[1–4]

In elemental ferromagnetic metals, the magnetostriction is relatively modest, for instance, about 46 ppm for Ni.[5] Table I summarizes the properties of typical magnetostrictive materials. Traditional magnetostrictive alloys such as Terfenol-D (Tb-Dy-Fe) and Galfenol (Fe–Ga) have demonstrated high strain levels (up to 1600 ppm at about 0.2 T), making them attractive for engineering applications.[6–8] However, their performance, inherent brittleness, high cost, or complex fabrication routes can limit their widespread adoption.

Beyond the conventional domain-rotation-driven magnetostriction, significantly larger effects can be achieved in materials that undergo a magnetic phase transition. When structural transformations are strongly coupled to the magnetic order, an applied magnetic field can induce abrupt lattice distortions or volume changes, resulting in magnetostrains that are several orders of magnitude greater than those generated by domain rotation alone (see Table I). These giant magnetostrains are especially prominent in intermetallic compounds that possess a large saturation magnetization. Representative families include FeRh,[9] $La(Fe,Si)_{13}$ alloys,[10–13] Laves phases,[14] MnCoSi or MnCoGe compounds,[15–18] MnAs,[19] $Gd_5Si_2Ge_2$,[20] and Heusler alloys,[21–24] all of which exhibit a first-order magnetic

TABLE I. Comparison of magnetostrictive materials with emphasis on systems based on first-order magnetic transition and giant shape memory effects. The "mechanism" indicates the origin of the magnetostrains or the nature of the phase transition.

Material	Magnetostrains (%)	Saturation field (T)	Coercivity /hysteresis (T)	Mechanism	Refs.
Terfenol-D	0.16	0.2	0.0025	Magnetic domain rotation	6
Galfenol	0.02	0.02	~0.0002	Magnetic domain rotation	7 and 8
FeRh	0.8	8	1.6	Isotropic magneto-elastic AF–FM transition	9
$La(Fe,Si)_{13}$	0.25	2	0.1	Isotropic magneto-elastic FM–PM transition	10–13
$(Hf,Ta)Fe_2$	0.4	5	0.1	Anisotropic FM–AFM magnetoelastic transition	14
$Co_{0.95}Ni_{0.05}MnSi$	0.6	6	0.5	Anisotropic AFM–FM magnetoelastic transition	15–17
$Mn_{0.98}CoGe$	0.05	5	⋯	Anisotropic FM–PM magnetostructural transition	18
MnAs	0.65	5	2.5	Anisotropic FM–PM magnetostructural transition	19
$Gd_5Si_2Ge_2$	0.2	2	0.5	Anisotropic FM–PM magneto-structural transition	20
Ni_2MnGa	9.5	1	1	Twin boundary motion	21 and 22
$Ni_{45}Co_5Mn_{36.6}In_{13.4}$	3	6	2.5	Martensitic transition	23 and 24

transition (FOMT). Although transition-driven magnetostrains offer a promising pathway toward an enhanced performance, they are frequently accompanied by drawbacks such as the need for high magnetic fields, a pronounced hysteresis, and reduced mechanical properties. These trade-offs must be carefully considered when evaluating such materials for practical applications. We can also note that, for most material systems, the magnetostrains are found to be significantly smaller than the volume change of the phase transition or the relative lattice parameter changes determined from XRD as a function of temperature or magnetic field. XRD probes the intrinsic unit-cell distortion at an atomic scale, whereas the macroscopically measured magnetostrains (strain gauge, tunneling tip, capacitance dilatometers, etc.) correspond to an effective macroscopic deformation of the entire sample, including the influence of the microstructure and the magnetic domains. For practical applications of polycrystalline materials, actual magnetostrictive measurements are needed to truly assess the potential of each magnetic phase transition.

MnFe(P,*X*) compounds with *X* = As, Ge, Si, or B are derived from the hexagonal Fe_2P parent system and form a rich materials family that has been intensively studied for its unusual FOMT and the associated giant magnetocaloric effect.[25–28] Contrary to most materials listed in Table I, the ferro-to-paramagnetic FOMT is not associated with a change in crystal symmetry or a sizable volume change. It, however, shows a nearly compensated contraction of the *a* axis and elongation of the *c* axis.[29,30] The proposed description for the FOMT implies distinct evolutions of the metal–metalloid distances for the non-equivalent 3*g* and 3*f* metal sites, corresponding

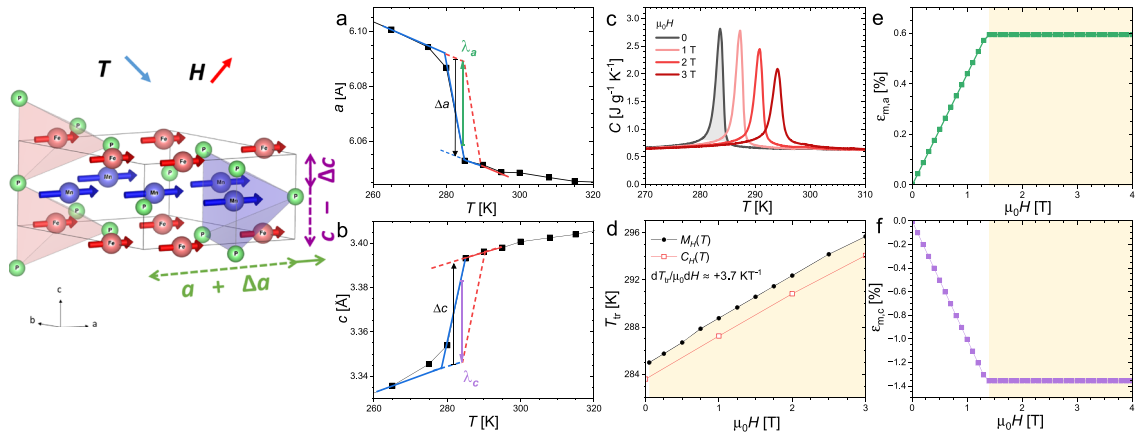

FIG. 1. Parametric estimate of the magnetostrains in Fe_2P-type compounds. (Left) Representation of the crystal structure of $(Mn,Fe)_2(P,Si)$ compounds highlighting the pyramidal and tetrahedral environments of Mn and Fe, respectively; the evolution of the lattice parameters upon cooling or magnetizing; and the a, b plane magnetization direction. Panels (a) and (b): Temperature evolution of the *a* and *c* lattice parameters of a $MnFe_{0.95}P_{0.585}B_{0.075}Si_{0.34}$ compound measured by XRD. The lines and arrows illustrate the discontinuities in lattice parameters and the construction used to estimate the magnetostrains (ε_m). Panels (c) and (d): Heat capacity measurements upon heating in various magnetic fields and evolution of the ferromagnetic transition as a function of the magnetic field, obtained from panel (b) and magnetization vs temperature curves. Panels (e) and (f): Calculated ε_m values from the parametric model along the a and c axes, respectively.

to pyramidal and tetrahedral metalloid environments, respectively (see illustration of the crystal structure in Fig. 1). The evolution of the interatomic distances influences the magnetic interactions; in particular, the decrease in the c/a ratio upon cooling favors ferromagnetism along with the development of a higher moment at the Fe 3f site. This leads to a cooperative mechanism where the magnetic, lattice, and electronic structures evolve simultaneously, resulting in an intense anisotropic FOMT.

As the FOMT involves anisotropic lattice discontinuities of opposite sign along the a and c axes, which nearly compensate each other, no significant macroscopic magnetostrains are in principle expected in randomly oriented polycrystalline bulk MnFe(P,X) samples. Yet, as demonstrated hereafter, large longitudinal magnetostrains can be obtained for textured materials. The texturation stage is dependent on the easy direction of the magnetic moments. The binary Fe_2P parent presents a strong uniaxial anisotropy with moments along the c axis;[29] whereas MnFe(P,Si) compounds show moments oriented along the a axis (in particular in Mn-rich compositions) or moments canted with respect to the c axis (with a canting angle of about 30°) at low Si contents, with anisotropy constants (K_1 and K_2) that are one order of magnitude weaker than for Fe_2P.[31–33]

To realize a proof of concept for magnetostrains in Fe_2P-type materials, we turned toward a composite approach, which usually combines magnetostrictive particles with polymeric, ceramic, or metallic matrices. These composites aim to balance the high magnetostrains of the active phase with the flexibility, toughness, and ease of processing provided by the matrix. Different fabrication strategies—such as particulate dispersion, laminated structures, and aligned fiber architectures—have been explored in the literature for other material families.[1–4] Yet the production of magnetostrictive composites uniquely depends on the active magnetic material and requires a specific development for each case. Section II presents a parametric model used to guide the selection of MnFe(P,Si,B) compounds. Section III describes the experimental methods and the development of a homemade dilatometer compatible with PPMS systems. Section IV shows and discusses the results on $MnFe_{0.95}P_{0.55}Si_{0.40}B_{0.05}$/epoxy composites demonstrating giant magnetostrains at intermediate magnetic fields.

II. MODELING MAGNETOSTRAINS AT THE FOMT OF MnFe(P,Si,B) COMPOUNDS

MnFe(P,X) compounds can present a broad range of magnetic properties at their ferromagnetic transition; in particular, compositional tuning allows a progression from a second-order magnetic transition (SOMT) to a FOMT with latent heat and giant discontinuities in cell parameters. The amplitude of the distortion has been observed to be linearly proportional to the strength of the FOMT, quantified as the latent heat (L).[34] We propose a parametric model relying on experimental measurements of the discontinuity in lattice parameters and of physical properties. This approach is a practical tool to estimate the maximum expected magnetostrains from existing experimental data on MnFe(P,X) compounds, thereby providing guidance for composition selection. The magnetostrain along the a and c axes of the hexagonal structure is defined as $\varepsilon_{m,a} = a(H)/a(0) - 1$ and $\epsilon_{m,c} = c(H)/c(0) - 1$, respectively.

The lattice discontinuities Δa and Δc should correspond to a step for an ideal FOMT. As illustrated in Fig. 1, in real materials, they are experimentally distributed over a narrow temperature range corresponding to the finite transition width δT_{tr}. Applying a magnetic field shifts the transition by $dT_{tr}/\mu_0 dH$, which can be measured directly or estimated from the Clausius–Clapeyron relation: $dT_{tr}/\mu_0 dH = -T_{tr}\Delta M/L$, where ΔM is the discontinuity in magnetization. This approach shares some similarities with several models that have been developed to estimate the isothermal entropy change and adiabatic temperature change in magnetocaloric materials.[35–39] Two regimes can be distinguished upon applying a magnetic field. When the transition is only partially induced, the magnetostrain along a given crystallographic direction is proportional to the magnetic field: $\varepsilon_{m,a} = -\frac{H\left(\frac{\Delta a}{a}\right)\left(\frac{dT_{tr}}{dH}\right)}{\delta T_{tr}}$. When the transition is fully induced at a critical field $H^* = \delta T_{tr}/\left(\frac{dT_{tr}}{dH}\right)$, the magnetostrain will saturate at $\varepsilon_{m,a} = -\Delta a/a$. The negative sign originates from the convention used to define the lattice discontinuities, Δa or Δc, which are usually estimated upon heating (ferro-to-paramagnetic transition). However, the magnetostrain upon magnetizing corresponds to the opposite transformation path.

This approach is presented in Fig. 1 for $MnFe_{0.95}P_{0.585}B_{0.075}Si_{0.34}$, a representative MnFe(P,X) compound developed for its giant magnetocaloric effect.[40–42] The shift of the transition under the field is clearly seen as the latent heat peak moves to higher temperatures. Notably, the transition broadens significantly only at higher fields (≥2 T), so assuming that δT_{tr} remains constant can be considered for intermediate fields. The value $dT_{tr}/\mu_0 dH = 3.7\ KT^{-1}$ may also be evaluated from $M(T)$ curves, and both methods yield a reasonable agreement. Large discontinuities in lattice parameters can be fully induced by magnetic fields of 1–2 T, leading to magnetostrains of about +0.4% along a and –1.0% along c for a field of 1 T, which is achievable using permanent magnets (or electromagnets). The lattice discontinuities being opposite in sign and nearly compensated, the net volume change $\varepsilon_{m,V} = 2\varepsilon_{m,a} + \varepsilon_{m,c}$ is anticipated to be negligible.

Although approximate, this model is well suited to guide materials selection. It highlights, for example, that targeting the largest unit-cell discontinuities is beneficial only above H^*. However, larger values of $\Delta a/a$ and $\Delta c/c$ are inevitably correlated with a larger latent heat, a broader hysteresis, and an increased embrittlement.[34] To maximize magnetostrains at intermediate fields ($H < H^*$)—most relevant for applications—it is important to increase the field sensitivity and minimize the transition width. Specifically for the Fe_2P family, since the lattice discontinuity correlates directly with L,[34] pursuing larger $\Delta a/a$ and $\Delta c/c$ necessarily reduces $dT_{tr}/\mu_0 dH$ at a fixed saturation magnetization. The strategies applied to optimize the MnFe(P,X) compounds for magnetocaloric performance—namely, tuning the transition toward the first-order/second-order boundary for the magnetic transition while maximizing the saturation magnetization to minimize hysteresis and maximize $dT_{tr}/\mu_0 dH$—are also highly relevant for optimizing magnetostrains at intermediate fields.

Since second-order transitions cannot concentrate large lattice parameter changes within a narrow temperature or field window, they appear unsuitable and were therefore not considered further. This view is supported by measurements on Fe_2(P,Si)/epoxy composites with a SOMT (see the supplementary material), which

exhibit magnetostrictive performances that are roughly an order of magnitude lower than the samples with a FOMT presented below.

III. EXPERIMENTAL DETAILS

The preparation of textured Fe_2P/epoxy composites consisted of several stages. First, bulk polycrystalline $MnFe_{0.95}P_{0.55}Si_{0.40}B_{0.05}$ compounds are synthesized by a solid-state reaction. Elemental powders were milled in a planetary mill for 10 h using a ball:sample ratio of 5:1. The resulting powders were pelletized into a cylinder, sealed into quartz ampules backfilled with 200 mbar Ar, and heat treated at 1100 °C for 24 h, ending with quenching in room temperature water. The pellet was then cooled to liquid N_2 temperature to remove the "virgin effect" (a training effect common to this family of materials), pulverized into powder by hand crushing in an agate mortar, and the powder was sieved below 36 μm. The sieving size was chosen based on previous investigations of closely related bulk materials prepared by the same method, which indicated an average grain size of ~24 μm.[40] The sieved powder is therefore expected to consist predominantly of single-grain particles. The composite is prepared by mixing weighted quantities of the sieved powder with epoxy (3M-DP270) and then poured into a cubic mold of 2 × 2 × 2 cm^3. The main text presents composites with an addition of +25 wt. % epoxy; different epoxy contents are presented in SM. For materials with easy axis orientation [$Fe_2(P,Si)$ compounds in the supplementary material], the magnetic orientation is achieved by inserting the mold into a static 1.1 T permanent magnet gap, whereas the cube was rotated at 60 rpm in the magnet gap for $MnFe_{0.95}P_{0.55}Si_{0.40}B_{0.05}$/epoxy samples with an easy plane anisotropy.

X-ray diffraction experiments were conducted on an Empyrean PANalytical diffractometer employing Cu-K_α radiation. Rietveld refinements showed that the main phase crystallizes in the Fe_2P-type structure, with lattice parameters close to those reported for closely related compositions.[40–42] As commonly observed in polycrystalline $(Mn,Fe)_2(P,Si)$ samples prepared by solid-state reaction, a cubic secondary phase with lattice parameters similar to Fe_3Si was also detected, amounting to about 2.3(6) wt. %. Physical properties were measured on a Quantum Design Dynacool 9 T system. Magnetic measurements were carried out using the vibrating sample magnetometer (VSM) option.

The linear thermal expansion $\alpha = (1/L)(dL/dT)$ and magnetostrains $\varepsilon_m = L(H)/L(0) - 1$ were measured using a homemade dilatometer option developed for the Quantum Design PPMS/Dynacool/Versalab system and based on the strain gauge method. The samples are mounted in the constant field region by using a copper holder fixed on a standard PPMS puck (see illustration in the supplementary material). Two identical strain gauges [BAB-120-3AA250(11), ZEMIC, Xi'an, China] were bonded with H-610 epoxy onto the sample and a fused silica reference and connected in a Wheatstone bridge circuit. A Keithley 2400 source unit provided the excitation voltage for the circuit, while the output signal was recorded by a Keithley 2182A nanovoltmeter. A LabVIEW virtual instrument was developed to simultaneously control the Quantum Design Dynacool through the Ethernet network and control/acquire the signals from the Keithley instruments connected by GPIB. Prior to the measurements, the reliability of this homemade setup was confirmed by measuring the linear thermal expansion of a high-purity copper sample (Puratronic, 99.999%, Alfa Aesar) mounted with strain gauges from the same batch. The measured linear thermal expansion for copper at 293 K was 16.8 ppm K^{-1}, in excellent agreement with the NIST standard value. Moreover, across a broad 50–350 K temperature range, the deviation of measured data from the NIST reference values did not exceed 2.5% (see the supplementary material), thereby validating the accuracy and reliability of our homemade dilatometer. Dilatometry measurements were carried out by sweeping the temperature at ±0.5 $Kmin^{-1}$ and magnetostrain measurements by sweeping the magnetic field at 0.42 $Tmin^{-1}$.

IV. RESULTS AND DISCUSSION

In the context of permanent magnet preparation, Fe_2P/epoxy composites with the *c* axis as the easy magnetization direction were successfully textured by applying a static magnetic field during composite processing.[43] For compositions with an easy magnetization direction in the *a*-*b* plane, magnetic texturing instead requires a rotating field to ensure alignment of the hard magnetic axis with the rotation direction.[44]

Figure 2 illustrates the orientation process and its confirmation through XRD and dilatometry measurements. It is important to note that, for a given face of the cube, XRD measurements are performed perpendicular to the face, whereas dilatometry is carried out with a strain gauge attached parallel to the face. On the XRD diffractograms, the face with a normal along the rotation direction shows a strong enhancement of the (001) and (002) diffraction peaks compared to a randomly oriented polycrystalline powder reference (data provided in the supplementary material), while the other main peaks with *a*, *b* components are strongly suppressed. This provides the first evidence that a significant texture was achieved in the composite by magnetic alignment. To assess the degree of orientation in the composite, the Lotgering factor method was used by comparing the relative peak intensities of powder XRD data for the oriented composite and that of the random powder.[45] The I_{00l} intensity was integrated over the ranges $25.5^\circ \le 2\theta \le 27^\circ$ (001) and $53.4^\circ \le 2\theta \le 55^\circ$ (002), whereas the I_{hkl} intensity was integrated over the $20^\circ \le 2\theta \le 90^\circ$ range (in both cases, a background estimated via spline interpolation was subtracted to account for the non-negligible sample fluorescence and the low-angle amorphous contribution from the epoxy). The resulting Lotgering factor, 0.83, is reasonably close to 1, indicating a strong, though not fully complete, texture, consistent with the still noticeable hkl and hk0 peaks visible in panel a of Fig. 2. We note that during the present magnetic orientation process, the epoxy was not diluted and remained relatively viscous; alternative magnetic orientation techniques (e.g., magnetic slip casting) may enable even higher texture levels.

Dilatometry experiments upon heating show a contraction typical of that observed along the *a* axis. This contraction upon heating is sharp at the transition temperature T_{tr} = 305 K and exhibits a thermal hysteresis of about 3–4 K, which are typical hallmarks of a first-order transition. The thermal contraction along this face corresponds to a negative thermal expansion (NTE) of about −0.36% in a 20 K temperature window, leading to an average linear thermal expansion coefficient $\alpha_a \approx -180$ ppm K^{-1} around the FOMT. While this NTE is significant and comparable in magnitude to

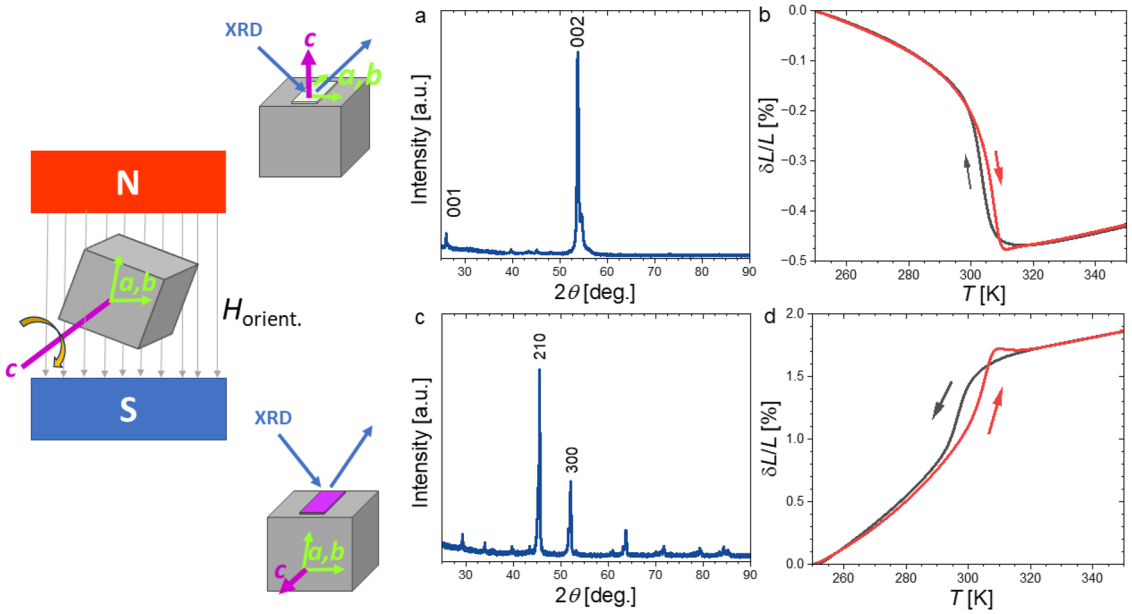

FIG. 2. Schematic representation of the magnetic field texturing for $MnFe_{0.95}P_{0.55}Si_{0.40}B_{0.05}$/epoxy composites and its characterization. The rectangular shape pasted along the cube faces marks out the position of the strain gauges. Panels (a) and (b): XRD along the rotation axis and dilatometry perpendicular to it. Panels (c) and (d): XRD perpendicular to the rotation axis and dilatometry parallel to it.

values reported for materials specifically designed to exhibit a giant-NTE,[46–48] it remains significantly less than the intrinsic contraction along the *a* axis (≈−0.6%), indicating that the epoxy matrix partly mitigates the intrinsic lattice contraction.

The four faces with normals aligned parallel to the rotating magnetic field show strongly enhanced (300) and (210) diffraction peaks, consistent with an easy magnetization direction along the *a* axis, characteristic of MnFe(P,Si) compounds with high Si content.[31–33] Dilatometry along the face shows a strong expansion typical of that observed along the *c* axis of the unit cell, with an amplitude nearly three times stronger than that observed along the *a* axis. The opposite and nearly compensated anisotropic linear thermal expansions yield a limited volume change, as previously pointed out by temperature dependent XRD measurements.[42]

Figure 3 shows magnetostrain measurements carried out longitudinally (with the magnetic field applied along the strain gauge) on the two different orientations of the cube. The cube face with the strain gauge aligned to the *a*-*b* plane, which contracts upon heating, leads to positive magnetostrains upon applying the magnetic field. The magnetostriction in the ferromagnetic state prior to the transition (250 K) is relatively limited and evolves nearly linearly at about 43 ppm T^{-1}. In the vicinity of the FOMT, giant magnetostrains appear due to the field-induced para-to-ferromagnetic transition. The magnetostrains are the largest just above the zero-field transition temperature, a temperature at which an intermediate magnetic field is sufficient to fully induce the transition, leading to magnetostrains of about 0.22% at 2 T and nearly saturating at 0.26% at 7 T. At higher temperatures, larger magnetic fields are required to induce the transition, resulting in smaller effects.

The cube face with the strain gauge aligned to the *c* axis, which expands upon heating, leads to negative magnetostrains upon applying the magnetic field. Similar to the previous orientation, giant magnetostrains develop in the close vicinity of the FOMT, but since the deformation of the active material is larger along the *c* axis than along *a*, the magnetostrains are larger, nearly saturating at −0.37% at 7 T.

In both cases, a finite magnetic field hysteresis is observed at the field-induced transition. However, it differs from that usually observed in field-induced magnetization curves for a FOMT (see magnetization measurements in the supplementary material). The magnetic field hysteresis is not only located in the field region of the FOMT but is also significant at the highest applied fields when the transition is fully induced (ferromagnetic phase fraction fully induced). The epoxy matrix affects the hysteresis of the materials mainly by providing a mechanical constraint, locking in local strains when reversing the magnetic field. Yet, in the intermediate field range (1 or 2 T), which is the most relevant for applications, the field hysteresis remains limited, for example, about 0.15 T in panel c of Fig. 3. This magnetic field range also corresponds to the field dependent regime of the model where the magnetostriction evolves nearly linearly at about −0.1%/T. Finally, we note that the perpendicular magnetostriction is of opposite sign to the longitudinal one, in line with the volume preserving nature of the FOMT.

In comparison with the magnetostrains predicted by the model in Sec. II, there is a qualitative agreement with the sign of the effect along the different orientations and with the existence of a critical field between 1 and 2 T above which the magnetostrains begin to saturate. Quantitatively, however, in $MnFe_{0.95}P_{0.55}Si_{0.40}B_{0.05}$/epoxy composites, one observes magnetostrains that are only one-third of

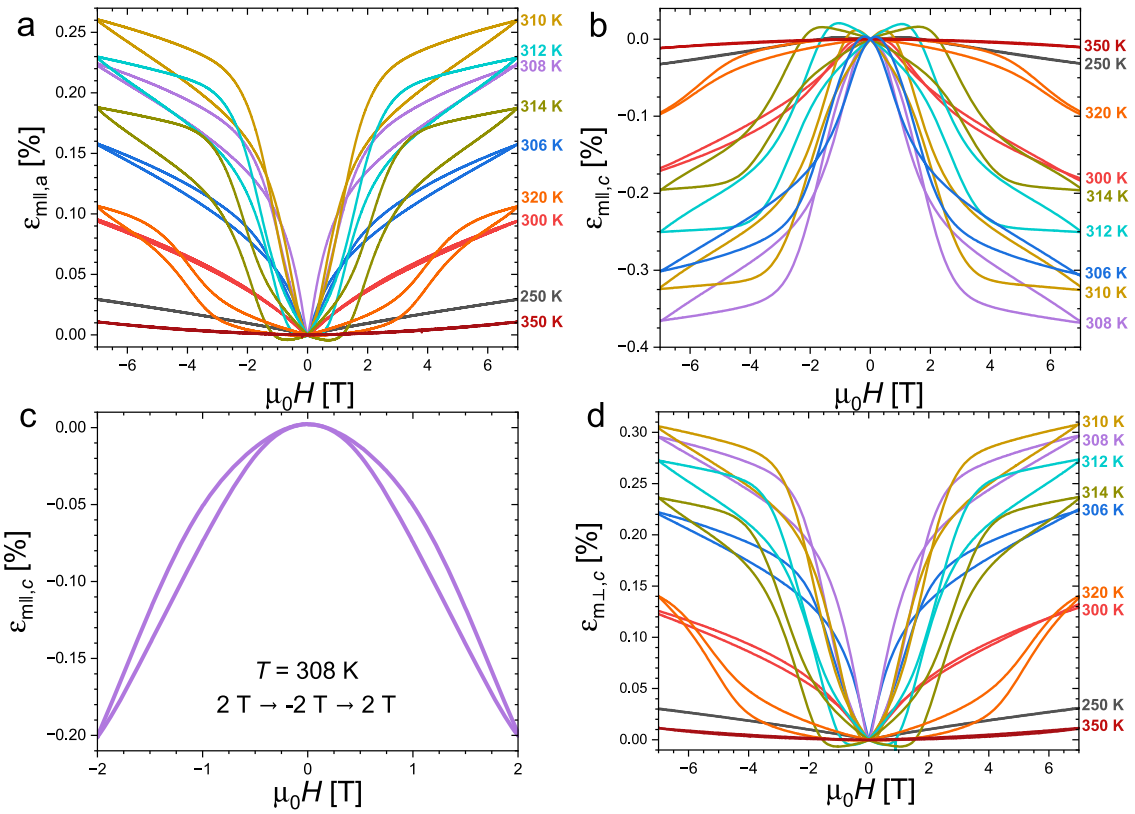

FIG. 3. Magnetostrains in $MnFe_{0.95}P_{0.55}Si_{0.40}B_{0.05}$/epoxy composites. Panel (a): Longitudinal magnetostrains with the strain gauge along the (a, b) plane [position equivalent to panel (b) of Fig. 2] recorded from 7 T to 7 T to 7 T at various temperatures. Panel (b): Longitudinal magnetostrains with a strain gauge along the c axis [position equivalent to panel (d) of Fig. 2] recorded from 7 T to 7 T to 7 T at various temperatures. Panel (c): Longitudinal magnetostrains with the strain gauge along the c axis recorded at T = 308 K with a 1 or 2 T maximum field. Panel (d): Perpendicular magnetostrains with a strain gauge along the c axis recorded from 7 T to 7 to 7 T at various temperatures.

those predicted by the model. Since the magnetostrains of the epoxy are negligible ($\varepsilon_{mEpoxy} \sim 0$), considering a basic rule of mixture for the effective magnetostrain of the composite $\varepsilon_m = f_{Epoxy}\varepsilon_{mEpoxy} + (1 - f_{epoxy})\ \varepsilon_{m(Mn,Fe)2(P,Si)} \approx (1 - f_{epoxy})\ \varepsilon_{m(Mn,Fe)2(P,Si)}$, the volume fraction of epoxy f_{Epoxy} acts as a dilution of the intrinsic magnetostrains of the $(Mn,Fe)_2(P,Si)$ main phase. In the present case, we chose to facilitate texturing over densification of the active phase by working with an added epoxy content of +25 wt. %, corresponding to a volume fraction of about 56 vol. % epoxy, larger than that traditionally used for magnetostrictive composites (30–50 vol. % fraction). This large epoxy content is responsible for most of the reduction in effective magnetostrains. In addition to the volume fraction, the softer epoxy will accommodate the magnetostrains from the Fe_2P material, and imperfect particle–matrix bonding will reduce the mechanical coupling, both further contributing to reduced effective transferred strains. Imperfect orientation, as pointed out in Fig. 2, may also contribute to reducing the effective magnetostrain of the composite. Finally, we note that in the case of the thermal expansion data presented in Fig. 2, the positive thermal expansion of the epoxy ($\alpha_{Epoxy} \approx 80\ ppmK^{-1}$) could not be neglected and would contribute to reducing the observed linear expansion anomalies along both orientations.

Despite the above limitations that are inherent to composites, we should point out that the present $MnFe_{0.95}P_{0.55}Si_{0.40}B_{0.05}$/epoxy samples possess some practical advantages compared to other magnetostrictive materials presented in Table I and, therefore, deserve further attention. Contrary to materials containing heavy rare earth, Ge, Rh, or As,[6,9,18–20] they are based on inexpensive, non-critical, and non-toxic raw materials. Heusler alloys with a martensitic transition can present magnetostrains significantly larger than presently observed, but often require a larger magnetic field to induce the transition.[23,24] In addition, the field hysteresis of the FOMT in Fe_2P compounds can be tuned to low values, which improves the reversibility of the effect. Actually, one great advantage of Fe_2P/composites is that they benefit from the efforts made in the search for materials with a cyclic giant magnetocaloric effect. By a subtle balance in the Mn:Fe ratio and the Si and B contents, MnFe(P,Si(,B)) compounds can be tuned to exhibit a FOMT with modest hysteresis in combination with a transition temperature that is tunable over a large temperature window, covering a temperature range from below to above room temperature.[26,42] While other transition-metal-based systems such as CoMnSi and $(Hf,Ta)Fe_2$ can present giant magnetostrains in bulk form without the need to process them as composites, their transition temperatures

cover a more limited temperature range; in particular, their giant magnetostrains develop below room temperature.[14–17] Finally, $La(Fe,Si)_{13}$ alloys and their hydrides exhibit magnetostrains of about 0.2% for 2 T in polycrystalline samples at room temperature, on par with what is presently observed, but they are relatively brittle in bulk form and are prone to dehydrating upon cycling through the FOMT. $La(Fe,Si)_{13}$/epoxy composites present an improved mechanical stability, but at the expense of nearly halved magnetostrains, ≈0.11% for 2 T.[49]

Collecting the present dataset (and performing some preliminary characterizations) required about 134 crossings of the phase transition as a function of temperature (from 250 to 350 K) or magnetic field (up to 7 T) on the same sample of $MnFe_{0.95}P_{0.55}Si_{0.40}B_{0.05}$/epoxy composite. No embrittlement of the sample or significant aging of its properties was observed. This behavior contrasts with bulk polycrystalline Fe_2P samples, which often develop (micro)cracks after only a few cycles across the phase transition, sometimes even leading to complete mechanical failure. The origin of this apparent mechanical stability of the composite likely includes (i) a high epoxy ratio (56 vol. %), which allows the composite to yield, and (ii) the texture, which helps limit the development of internal stresses, in contrast to polycrystalline bulk samples, where the opposite lattice parameter discontinuities can create large local stresses at grain boundaries. Dedicated mechanical investigations will be required to compare more quantitatively bulk and composite samples.

V. CONCLUSIONS

A practical method has been implemented to shape and texture Fe_2P-compounds/epoxy composites. The thermal expansion and magnetostrains of $MnFe_{0.95}P_{0.55}Si_{0.40}B_{0.05}$/epoxy composites were studied as a function of temperature and magnetic field. We show that the anisotropic character of the transition and the low magnetic anisotropy do not hinder the realization of large linear magnetostrains, reaching up to 0.1%/T at intermediate magnetic fields. A parametric model indicates that the composition selection of the active phase should focus on materials exhibiting a sharp first-order magnetic transition with a large field sensitivity, particularly in the intermediate field region (1–2 T). In the field of magnetocaloric applications, discontinuities in lattice parameters at the ferromagnetic transition are undesirable and pose serious technical challenges for integrating these materials into functional systems. Conversely, we show that when texturing is applied, these lattice discontinuities can be exploited to achieve large magnetostrains, thereby opening this material family to a new field of application. Owing to the large temperature range achievable by chemical compounding of the active phase and the limited transition hysteresis ensuring reversibility of the effect, this proof of concept establishes Fe_2P/epoxy composites as a promising class of magnetostrictive materials derived from abundantly available, low-cost elements.

SUPPLEMENTARY MATERIAL

The supplementary material includes additional figures illustrating (i) dilatometry measurements on a Cu standard, (ii) the thermal expansion and magnetostrains of a composite with a second-order transition, (iii) magnetization measurements, and (iv) the XRD data for the randomly oriented powder.

ACKNOWLEDGMENTS

This study was supported by the National Natural Science Foundation of China (Grant Nos. 12464015 and 52461036) and the program for young talents of science and technology in the universities of the Inner Mongolia Autonomous Region (Grant No. NJYT23107). The position of F. Guillou at Caen University is supported by the French government, managed by the Agence Nationale de la Recherche under the France 2030 program, under the Reference No. ANR-23-EXES-0001, by the Normandy region, and by a CPJ project.

AUTHOR DECLARATIONS

Conflict of Interest

The authors have no conflicts to disclose.

Author Contributions

B. Huhe: Data curation (equal); Investigation (equal). **H. Yibole**: Project administration (equal); Supervision (equal); Writing – review & editing (equal). **F. Guillou**: Conceptualization (equal); Formal analysis (equal); Visualization (equal); Writing – original draft (equal). **N. H. van Dijk**: Supervision (equal); Validation (equal); Writing – review & editing (equal). **E. Brück**: Supervision (equal); Validation (equal); Writing – review & editing (equal).

DATA AVAILABILITY

The data that support the findings of this study are available from the corresponding author upon reasonable request.

REFERENCES

[1] G. Engdahl, *Handbook of Giant Magnetostrictive Materials* (Academic Press, 2000).
[2] A. G. Olabi and A. Grunwald, Mater. Des. **29**, 469–483 (2008).
[3] Z. Deng and M. J. Dapino, Smart Mater. Struct. **27**, 113001 (2018).
[4] C. Gao, Z. Zeng, S. Peng, and C. Shuai, Bioact. Mater. **8**, 177–195 (2022).
[5] E. W. Lee, Rep. Prog. Phys. **18**, 184 (1955).
[6] H. T. Savage, R. Abbundi, A. E. Clark, and O. D. McMasters, J. Mag. Mag. Mater. **15**, 609 (1980).
[7] A. E. Clark, J. B. Restorff, M. Wun-Fogle, T. A. Lograsso, and D. L. Schlagel, IEEE Trans. Magn. **36**, 3238 (2000).
[8] V. Milyutin, R. Bureš, and M. Fáberová, Condens. Matter **8**, 80 (2023).
[9] M. R. Ibarra and P. A. Algarabel, Phys. Rev. B **50**, 4196 (1994).
[10] S. Fujieda, A. Fujita, K. Fukamichi, Y. Yamazaki, and Y. Iijima, Appl. Phys. Lett. **79**, 653–655 (2001).
[11] N. Z. Abdulkadirova, A. G. Gamzatov, K. I. Kamilov, A. T. Kadirbardeev, A. M. Aliev, Y. F. Popov, G. P. Vorob'ev, and P. Gebara, J. Alloys Compd. **929**, 167348 (2022).
[12] S. Li, R. Huang, Y. Zhao, W. Wang, Y. Han, and L. Li, Adv. Funct. Mater. **27**, 1604195 (2016).
[13] Y. Song, R. Huang, Y. Liu, Z. Zhang, Q. Huang, Y. Jiang, S. Wang, L. Li, X. Xing, and J. Chen, Chem. Mater. **32**, 7535 (2020).

[14]G. Kido, Y. Tadakuma, Y. Nakagawa, Y. Nishihara, and Y. Yamaguchi, J. Mag. Mag. Mater. **54**, 885 (1986).
[15]A. Barcza, Z. Gercsi, K. S. Knight, and K. G. Sandeman, Phys. Rev. Lett. **104**, 247202 (2010).
[16]X. Hao, B. Yang, J. Li, D. Wang, Z. Li, H. Yan, Y. Zhang, C. Esling, X. Zhao, and L. Zuo, Acta Mater. **242**, 118486 (2023).
[17]J. Liu, Y. Gong, F. Zhang, Y. You, G. Xu, X. Miao, and F. Xu, J. Mater. Sci. Technol. **76**, 104–110 (2021).
[18]F. Zhu, J. Lin, X. Zhang, L. Li, C. Yang, M. Wang, Y. Wu, P. Tong, W. Song, and Y. Sun, J. Alloys Compd. **782**, 881 (2019).
[19]V. A. Chernenko, L. Wee, P. G. McCormick, and R. Street, J. Appl. Phys. **85**, 7833–7837 (1999).
[20]M. Han, D. C. Jiles, J. E. Snyder, T. A. Lograsso, and D. L. Schlagel, J. Appl. Phys. **95**, 6945–6947 (2004).
[21]K. Ullakko, J. K. Huang, C. Kantner, R. C. O'Handley, and V. V. Kokorin, Appl. Phys. Lett. **69**, 1966 (1996).
[22]A. Sozinov, A. A. Likhachev, N. Lanska, and K. Ullakko, Appl. Phys. Lett. **80**, 1746–1748 (2002).
[23]R. Kainuma, Y. Imano, W. Ito, Y. Sutou, H. Morito, S. Okamoto, O. Kitakami, K. Oikawa, A. Fujita, T. Kanomata, and K. Ishida, Nature **439**, 957–960 (2006).
[24]L. Mañosa, X. Moya, A. Planes, T. Krenke, M. Acet, and E. F. Wassermann, Mater. Sci. Eng. A. **481–482**, 49–56 (2008).
[25]O. Tegus, E. Brück, K. H. J. Buschow, and F. R. de Boer, Nature **415**, 150–152 (2002).
[26]N. H. Dung, Z. Q. Ou, L. Caron, L. Zhang, D. T. C. Thanh, G. A. de Wijs, R. A. de Groot, K. H. J. Buschow, and E. Brück, Adv. Energy Mater. **1**, 1215 (2011).
[27]F. Zhang, P. Feng, A. Kiecana, Z. Wu, Z. Bai, W. Li, H. Chen, W. Yin, X. W. Yan, F. Ma, N. v. Dijk, E. Brück, and Y. Ren, Adv. Funct. Mater. **34**, 2409270 (2024).
[28]A. Y. Lee, K. H. Kang, S. C. Park, and J. W. Kim, APL Mater. **11**, 091103 (2023).
[29]H. Fujii, T. Hōkabe, T. Kamigaichi, and T. Okamoto, J. Phys. Soc. Jpn. **43**, 41–46 (1977).
[30]L. Lundgren, G. Tarmohamed, O. Beckman, B. Carlsson, and S. Rundqvist, Phys. Scr. **17**, 39–48 (1978).
[31]H. Yibole, F. Guillou, Y. K. Huang, G. R. Blake, A. J. E. Lefering, N. H. van Dijk, and E. Brück, Appl. Phys. Lett. **107**, 162403 (2015).
[32]N. H. Dung, L. Zhang, Z. Q. Ou, L. Zhao, L. van Eijck, A. M. Mulders, M. Avdeev, E. Suard, N. H. van Dijk, and E. Brück, Phys. Rev. B **86**, 045134 (2012).
[33]Z. Q. Ou, L. Zhang, N. H. Dung, L. van Eijck, A. M. Mulders, M. Avdeev, N. H. van Dijk, and E. Brück, J. Magn. Magn Mater. **340**, 80 (2013).
[34]F. Guillou, H. Yibole, B. Narsu, and V. Hardy, Results Phys. **44**, 106203 (2023).
[35]V. Pecharsky, K. Gschneidner, A. Pecharsky, and A. Tishin, Phys. Rev. B **64**, 144406 (2001).
[36]K. G. Sandeman, Scr. Mater. **67**, 566–571 (2012).
[37]G. Porcari, S. Fabbrici, C. Pernechele, F. Albertini, M. Buzzi, A. Paoluzi, J. Kamarad, Z. Arnold, and M. Solzi, Phys. Rev. B **85**, 024414 (2012).
[38]V. Recarte, J. I. Pérez-Landazábal, S. Kustov, and E. Cesari, J. Appl. Phys. **107**, 053501 (2010).
[39]J. Liu, T. Gottschall, K. P. Skokov, J. D. Moore, and O. Gutfleisch, Nat. Mater. **11**, 620 (2012).
[40]B. Suye, H. Yibole, Z. Q. Song, B. Tana, W. Wei, O. Haschuluu, O. Tegus, and F. Guillou, J. Alloys Compd. **976**, 172918 (2024).
[41]J. Y. Xu, F. Guillou, H. Yibole, and V. Hardy, Fundam. Res. **4**, 1465 (2024).
[42]F. Guillou, G. Porcari, H. Yibole, N. van Dijk, and E. Brück, Adv. Mater. **26**, 2671–2675 (2014).
[43]H. Yibole, B. Lingling-Bao, J. Y. Xu, H. Alata, O. Tegus, W. Hanggai, N. H. van Dijk, E. Brück, and F. Guillou, Acta Mater. **221**, 117388 (2021).
[44]W. Qun, Z. Zhi-gang, L. Wei, X. K. Sun, Y. C. Chuang, and F. R. de Boer, J. Mag. Mag. Mater. **109**, 59–63 (1992).
[45]F. Lotgering, J. Inorg. Nucl. Chem. **9**, 249–254 (1959).
[46]A. W. Sleight, Curr. Opin. Solid State Mater. Sci. **3**, 128–131 (1998).
[47]K. Takenaka, Sci. Technol. Adv. Mater. **13**, 013001 (2012).
[48]Q. Li, K. Lin, Z. Liu, L. Hu, Y. Cao, J. Chen, X. Xing, J. Chen, and X. Xing, Chem. Rev. **122**, 8438–8486 (2022).
[49]K. Matsumoto, D. Murayama, M. Takeshita, Y. Ura, S. Abe, T. Numazawa, H. Takata, Y. Matsumoto, and T. Kuriiwa, J. Phys. Conf. **897**, 012011 (2017).